

Space Weather®

RESEARCH ARTICLE

10.1029/2024SW004005

Key Points:

- The Weimer Geomagnetic Perturbation Model is evaluated for real-time prediction of geomagnetic disturbances at high latitudes
- The Weimer model reduces geomagnetic reference errors at high latitudes by 20%–30% based on comparisons to observatory data
- Measurement-while-drilling data show that the Weimer model can save valuable rig time by reducing geomagnetic reference model errors

Correspondence to:

S. Califf,
califf@colorado.edu

Citation:

Califf, S., Nair, M., Weimer, D., Zachman, N., & Poedjono, B. (2024). Assessment of the Weimer geomagnetic perturbation model for high-latitude positioning and navigation. *Space Weather*, 22, e2024SW004005. <https://doi.org/10.1029/2024SW004005>



Received 20 MAY 2024

Accepted 5 OCT 2024

Author Contributions:

Conceptualization: S. Califf, M. Nair, N. Zachman, B. Poedjono
Formal analysis: S. Califf, N. Zachman, B. Poedjono
Methodology: S. Califf, M. Nair, D. Weimer, N. Zachman, B. Poedjono
Software: S. Califf, D. Weimer
Supervision: M. Nair
Writing – original draft: S. Califf
Writing – review & editing: S. Califf, M. Nair, D. Weimer, N. Zachman, B. Poedjono

Assessment of the Weimer Geomagnetic Perturbation Model for High-Latitude Positioning and Navigation

S. Califf^{1,2} , M. Nair^{1,2}, D. Weimer³ , N. Zachman⁴, and B. Poedjono⁵

¹Cooperative Institute for Research in Environmental Sciences, Boulder, CO, USA, ²National Centers for Environmental Information, Boulder, CO, USA, ³Center for Space Science and Engineering Research, Virginia Tech (Retired), Blacksburg, VA, USA, ⁴K&M Technologies, Denver, CO, USA, ⁵BPH Consulting, Sugar Land, TX, USA

Abstract The Geomagnetism Group at the National Centers for Environmental Information (NCEI), in collaboration with the Cooperative Institute for Research in Environmental Sciences (CIRES), along with various government and industry partners, specializes in developing and providing access to Earth's internal magnetic field models. These models are crucial for applications such as compass navigation and wellbore positioning, offering reference values for the geomagnetic field (total field, dip or inclination, and declination) at any location across the Earth. This study assesses the Weimer geomagnetic perturbation model, proposed by Weimer in 2013, which is an empirical model of magnetic field variations at high latitudes driven by solar wind measurements, as a candidate for capturing geomagnetic field variations in high-latitude areas. We compare the geomagnetic field variations predicted by the Weimer model against data from the INTERMAGNET and SuperMAG observatory networks. Our findings indicate that the Weimer model achieves a reduction in the standard deviations of high-latitude magnetic field variations by approximately 20%–30% once quiet-time baselines are removed from the data set. Furthermore, we compare the performance of the Weimer model against the Space Weather Modeling Framework's Geospace model during specific geomagnetic storms in 2017 and 2018, and we find that the Weimer model is more effective in predicting magnetic variations at high latitudes than the Geospace model during these storms. Additionally, comparisons to magnetometer data collected from high-latitude directional-drilling operations align with the trends observed in comparisons with INTERMAGNET and SuperMAG observatory data, confirming the Weimer model's reliability and effectiveness for such applications.

Plain Language Summary The Geomagnetism Group at the National Centers for Environmental Information (NCEI), in collaboration with the Cooperative Institute for Research in Environmental Sciences (CIRES), along with various government and industry partners, develops geomagnetic models that are used for navigation and oil drilling applications. At high latitudes, geomagnetic variations caused by the interaction between the solar wind and the Earth's magnetic field increases uncertainty in the models. This study assesses the Weimer geomagnetic perturbation model as a candidate to compensate for these geomagnetic variations. We compare the model to scientific ground observatories, and show that the model captures 20%–30% of the variation. We also demonstrate that the model is useful in applied setting by comparing the model to data collected from oil drilling operations.

1. Introduction

The Earth's magnetic field can be represented as a superposition of the core field, the crustal field, and external fields of ionospheric and magnetospheric origin. The High Definition Geomagnetic Model (HDGM) (Nair et al., 2021) uses a spherical harmonic description of the main and crustal fields to degree and order 790 derived from many years of satellite magnetic field measurements by the Swarm mission, providing geomagnetic reference values for applications such as compass navigation and directional drilling for wellbore positioning. Directional drillers rely on the Earth's magnetic and gravity fields as natural references for the azimuth and inclination of the drill bit's bottom hole assembly (BHA). To accurately estimate position, drillers use gravity and magnetic sensors within their Measurement While Drilling (MWD) tools, combining raw magnetic measurements with knowledge of the local geomagnetic field strength and direction from a geomagnetic reference model such as HDGM.

Errors in the geomagnetic reference model are a significant source of inaccuracy in determining borehole trajectory, as the local geomagnetic field measured by sensors comprises various sources including the core, crustal

© 2024. The Author(s).

This is an open access article under the terms of the [Creative Commons Attribution License](https://creativecommons.org/licenses/by/4.0/), which permits use, distribution and reproduction in any medium, provided the original work is properly cited.

field, and space-weather related fields. The accuracy of these geomagnetic reference models, which estimate the vector components of the geomagnetic field, is crucial for minimizing the ellipsoid of uncertainties (EOUs) in borehole trajectory, allowing for tighter placement of adjacent boreholes. The HDGM represents the slowly varying core field ($n \leq 15$), the relatively constant crustal field ($n > 15$), and it includes an annually averaged external field model. A real-time version of HDGM (HDGM-RT) also includes a symmetric ring current model driven by solar wind measurements at Sun-Earth L1 (Maus & Lühr, 2005) and an ionospheric model of diurnal variations (Chulliat et al., 2016).

This study evaluates the Weimer geomagnetic perturbation model (Weimer, 2013), hereafter referred to as WGPM, as a candidate for inclusion in HDGM-RT to predict high-latitude (magnetic latitude $>55^\circ$) geomagnetic disturbances on the Earth's surface in real time. There is a corresponding Weimer electric potential model (Weimer, 2005) that is widely used for simulations of the Earth's magnetosphere. High-latitude geomagnetic disturbances are generated by magnetospheric currents and field-aligned currents that are diverted and close horizontally through the ionosphere, and are ultimately a result of external driving by the solar wind. Geomagnetic perturbations measured on the ground are also affected by ground conductivity by up to $\sim 30\%$ (Pulkkinen & Engels, 2005). WGPM is an empirical model of high-latitude geomagnetic disturbances derived from ground observatory data, so the model implicitly includes the effects of magnetospheric currents, ionospheric currents, and ground conductivity. The model is driven by solar wind measurements at the Sun-Earth L1 Lagrange point, which is a stable orbit located between the Earth and the Sun ($\sim 1\%$ of the distance to the Sun), providing approximately 45 min of lead time between the input observations and the geomagnetic perturbation on the Earth's surface.

Previous studies of the predictive performance of geomagnetic field perturbation models mostly focused on dB/dt , which is of interest to the space weather community due to hazards to the power grid associated with geomagnetically induced currents (GIC) (e.g., Anderson et al., 1974; Boteler et al., 1998). Pulkkinen et al. (2013) evaluated several models, including an earlier version of WGPM (Weimer et al., 2010), for operational use by NOAA SWPC to predict dB/dt by comparing the models to data from 12 observatories for 6 geomagnetic storms. This study and a follow-up study by Welling et al. (2018) found that WGPM, as well as the other candidate models, tended to underpredict the observed dB/dt during the selected geomagnetic storms. Al Shidi et al. (2022) compared the Space Weather Modeling Framework (SWMF) Geospace model, which was ultimately selected as the operational model for SWPC, to measurements of the horizontal and vertical components of the magnetic field perturbations from the SuperMAG database for 122 geomagnetic storms between 2010 and 2019. The study found that the Geospace model performance was degraded at high latitudes.

Our focus is to evaluate the ability of WGPM to improve geomagnetic field estimates at high latitudes for geomagnetic referencing applications (e.g., Buchanan et al., 2013), so we examine all three components of the geomagnetic perturbations (in geographic North-East-Center (NEC) coordinates) and the impact these have on estimates of total field (F), declination (D), and dip or inclination (I). We also leverage Geospace simulation results from the Al Shidi et al. (2022) study to compare WGPM to the Geospace model (Al Shidi & Pulkkinen, 2022), as the Geospace model could also potentially be used for real-time estimates of geomagnetic perturbations for navigation. The observatory data, WGPM, and Geospace model are described in Section 2, and Section 3 presents the methodology used to evaluate the models. In Section 4, WGPM is evaluated relative to high-latitude INTERMAGNET data, and total uncertainty is derived including HDGM baseline errors. WGPM is compared to the Geospace model for several geomagnetic storms in Section 5, and Section 6 demonstrates the applicability of the model to MWD data collected from high-latitude drilling operations. Section 7 provides the conclusions of the study.

2. Observatory Data and Geomagnetic Field Models

2.1. INTERMAGNET and Observatory Data

We used one-minute data from the INTERMAGNET (Kerridge, 2001) and SuperMAG (Gjerloev, 2012) observatory networks to evaluate the performance of WGPM at locations above 55° magnetic latitude in the northern hemisphere. The observatory locations are plotted in Figure 1. We used definitive INTERMAGNET which include calibrated baselines maintained by the British Geological Survey (BGS) (Macmillan & Olsen, 2013). SuperMAG data processing applies a variable time window to remove observatory baselines based on the most “common” measurement, and many of the SuperMAG observatories only record variations in the

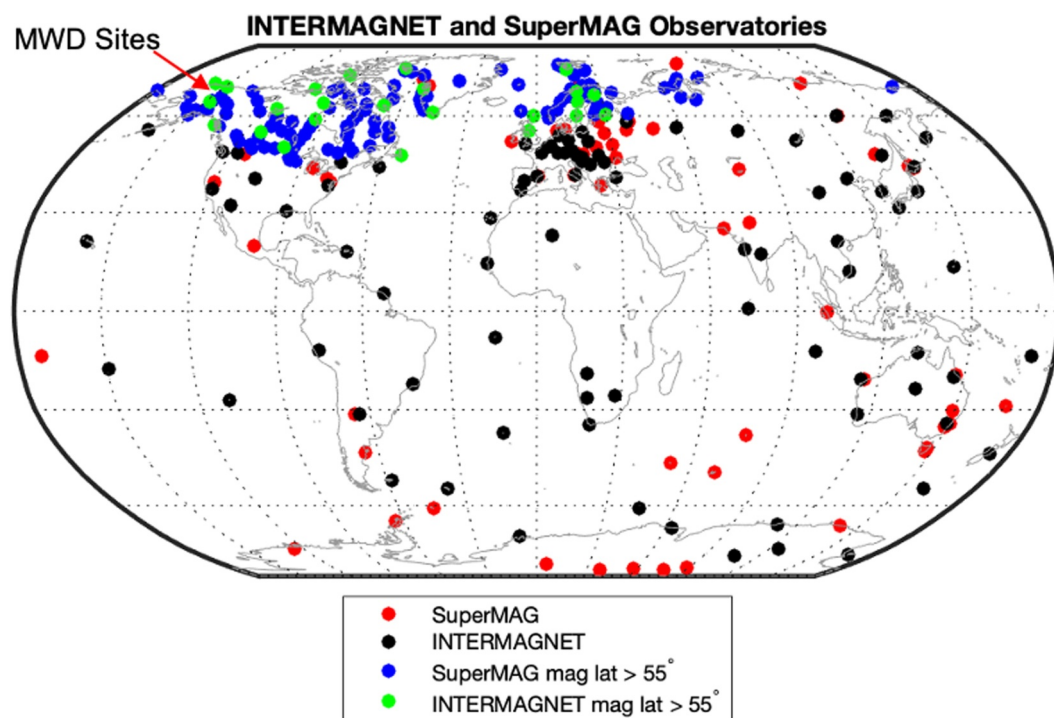


Figure 1. INTERMAGNET and SuperMAG observatory locations.

geomagnetic field. We use definitive INTERMAGNET data to evaluate the performance of WGPM during 2017–2018 in estimating total field, declination, and inclination, and SuperMAG data are used in a comparison to the Geospace model for several geomagnetic storms.

2.2. Weimer Geomagnetic Perturbation Model

WGPM uses 5-min measurements of the interplanetary magnetic field (IMF) and solar wind velocity at Sun–Earth L1, the dipole tilt angle, and the F10.7 index as inputs to estimate the deviation in the geomagnetic field on the Earth's surface. The input data are delayed by 20 min to account for the propagation delay between the Earth's bow shock and the ground through the magnetosphere, and the 5-min data are further averaged by 25 min based on empirical testing of the correlation between the IMF and ground observations. The model represents the geomagnetic perturbations with spherical cap harmonics, where the coefficients are nonlinear functions of the input parameters that were determined by trial and error to achieve the best fit to many years of ground observatory data. We evaluated the model at one-minute intervals at the INTERMAGNET and SuperMAG observatories located above 55° magnetic latitude to compare with one-minute observational data. The power spectrum of magnetic perturbations has been shown to significantly decrease on timescales shorter than 1 minute (Pulkkinen et al., 2006).

2.3. Geospace Model

The Geospace model is a physics-based model that couples the BATS-R-US outer magnetospheric model (Gombosi et al., 2004), the Rice Convection Model (RCM) inner magnetospheric model (Toffoletto et al., 2003), and the Ridley Ionosphere Model (RIM) (Ridley et al., 2004). The Space Weather Modeling Framework (SWMF) is a version of the Geospace model employed by NOAA SWPC to create operational ground magnetic perturbation maps. We use one-minute model outputs of the SWMF version of the Geospace model for several geomagnetic storms in 2017 and 2018 produced by Al Shidi et al. (2022) to compare to WGPM. The model was evaluated at SuperMAG observatories, and we focused on the observatories located above 55° magnetic latitude.

3. Methodology

In navigation applications, magnetic field measurements are compared to reference models, such as HDGM, to derive pointing information. The reference model is assumed to be truth, so errors in the reference model directly cause errors in the pointing estimate. The HDGM includes geomagnetic sources from the Earth's core and lithospheric fields, but it does not model perturbations related to geomagnetic activity. Our goal is to evaluate how well the WGPM can estimate geomagnetic perturbations, and ultimately to compensate for geomagnetic perturbations in HDGM to reduce pointing errors. We compute the compensated residuals by subtracting the WGPM prediction from observatory measurements of geomagnetic perturbations, which we call "WGPM-compensated" data. This residual represents the error in the geomagnetic reference model after compensating using WGPM. The raw observatory residuals represent the geomagnetic reference model error without WGPM compensation. We compare the standard deviations of the compensated and raw observatory data over a 2-year period to evaluate the model performance, where a reduction in the compensated residual standard deviation reflects a smaller geomagnetic reference model error and improved pointing estimates.

4. WGPM-INTERMAGNET Comparison

We compare WGPM to geomagnetic variations measured by 25 observatories located above 55° magnetic latitude from the INTERMAGNET network during 2017 and 2018. Here we are interested in the observed variations (minutes to hours) about the slowly varying (on the order of years) baseline geomagnetic field originating from the Earth's core and crust. Baselines for each observatory were estimated by fitting a static offset, linear secular variation, and a sine wave with a 6-month period to hourly averaged data selected during geomagnetically quiet periods based on the Kp index (Bartels, 1949), the IMF, and the ring current index (RC) (Olsen et al., 2014). The quiet-time criteria were:

- $K_p \leq 2$
- IMF Bz [−5, 0] nT
- IMF By [−6, 6] nT
- $dRC/dt < 3$ nT/hr
- Local time between 1 and 5

An example of the baseline fit for the Eskdalemuir observatory (ESK, 55.3°N, 356.8°E) is shown in Figure 2. The baseline curve parameters were estimated using an iterative least-squares fit, where one-sigma outliers were removed in three iterations to address visible biases due to the outliers.

Figure 3 shows an example of the measurement at the Hornsund observatory (HRN, 77°N, 15.6°E) with the baseline removed compared to WGPM prediction for a geomagnetic storm on 2017-05-28. The three days leading up to the storm were geomagnetically quiet ($K_p < 1$), and the quiet-time daily variations related to the Sq current system (e.g., Yamazaki & Maute, 2017) are generally captured by WGPM. The variations increase to several hundred nT during the geomagnetic storm on 2017-05-28, return to the quiet-time pattern, and then increase again when a smaller storm arrives on 2017-05-29. WGPM predicts part of the slower trends during the geomagnetically active periods, but does not capture the higher-frequency variations present in the 1-min data due to the 25-min moving average on solar wind input data in the model. The model more closely matches the E and C components of the active-time geomagnetic variations, although there is an apparent small phase lead in both of these components.

Standard deviations for the measurements and measurement residuals relative to WGPM in geographic NEC coordinates are shown in Figure 4. Results for all of the data from 2017 to 2018 are plotted with closed circles, and storm-time data ($K_p \geq 4$) are plotted with open circles. The measured N component variations (blue) increase with magnetic latitude up to ~65°, and then decrease at magnetic latitudes above 70°, while the E and C component variations are largest between 70° and 75°. During active times (open circles), the standard deviations of the raw observations increase by a factor of 3–4, and the trends with magnetic latitude remain intact. The red circles are standard deviations for the measurement with WGPM subtracted, which reflects the errors if WGPM were used in real-time to compensate for the geomagnetic disturbances. The smaller standard deviations for the WGPM residuals indicate that the model captures part of the observed variation, with larger improvements occurring during

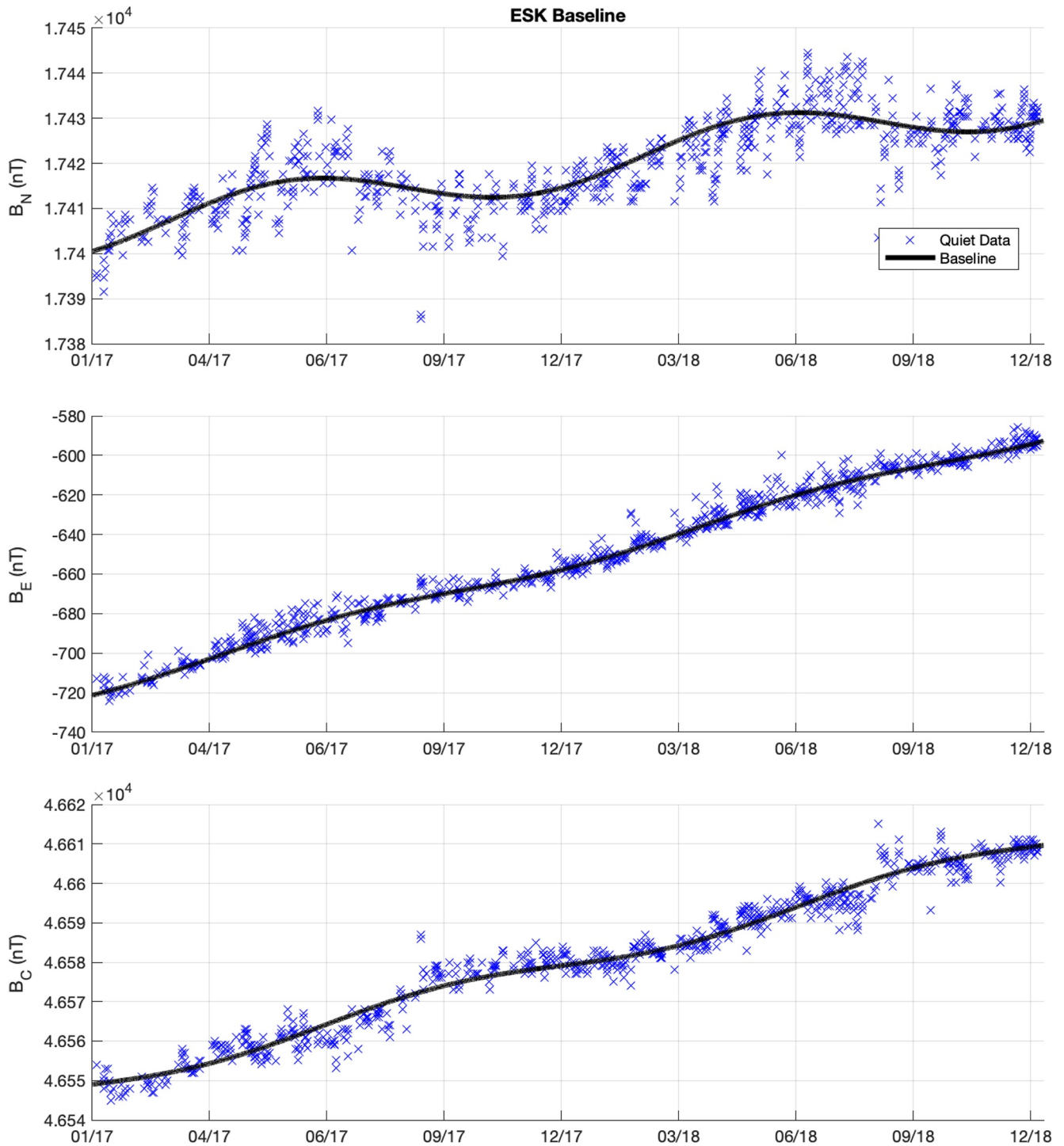


Figure 2. Baseline fit to quiet-time data for the ESK observatory in North-East-Center (NEC) coordinates.

storm-time when the geomagnetic field disturbances are greater. WGPM performs better between 60° and 70° magnetic latitude for the N component, and 70° – 80° magnetic latitude for the E and C components. 2017–2018 was not a particularly active period (see Figure 7); the storm-time data account for only 6.4% of the total data set (1,116 hours) and there were only 3 storms with minimum Dst below -100 nT. These results represent moderate

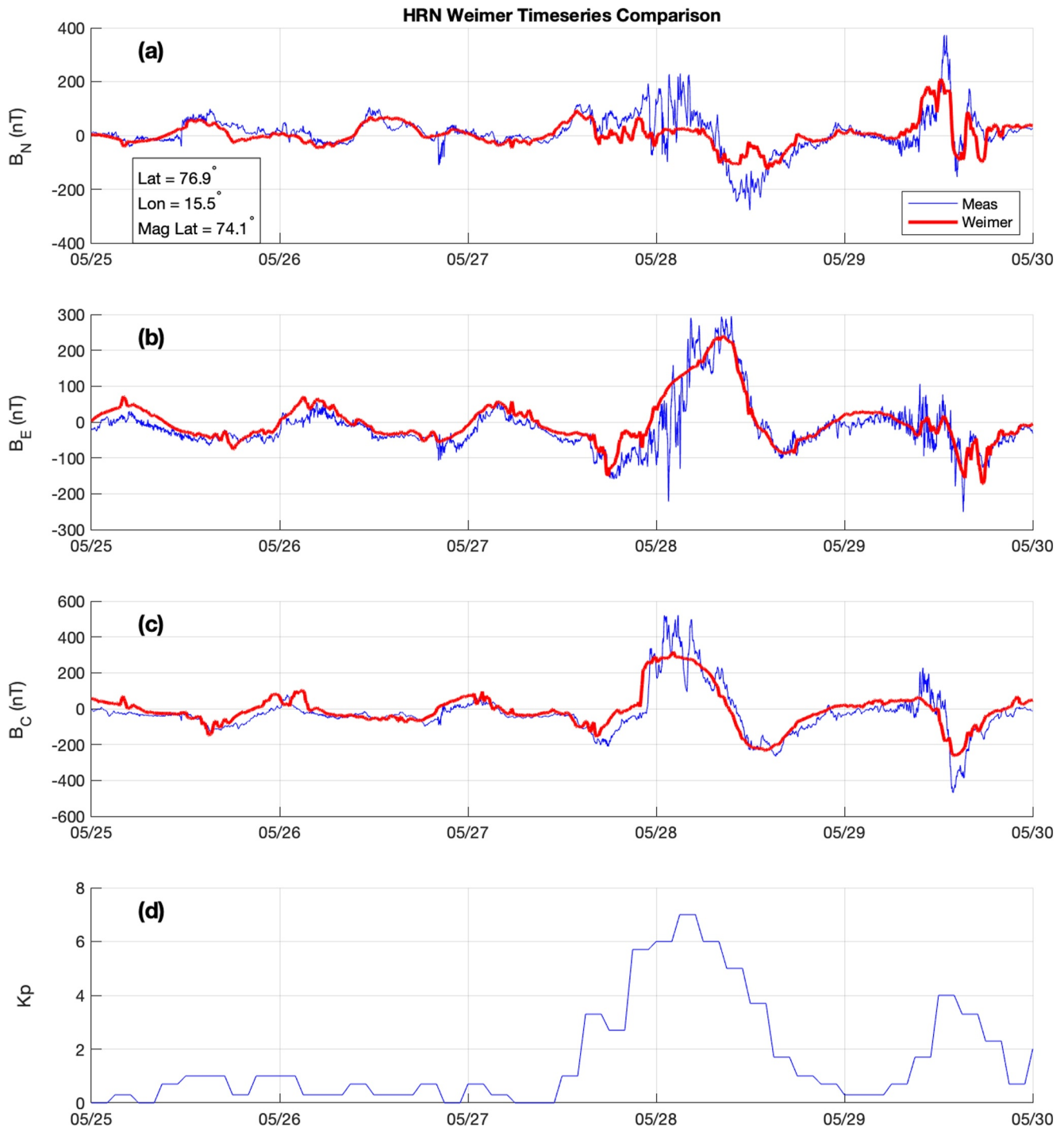


Figure 3. Timeseries of the measured magnetic field at HRN with baseline removed and WGPM for a quiet period leading to a geomagnetic storm in May 2017. (a) North, (b) East, (c) Center magnetic field variations, and (d) Kp index.

geomagnetic activity, and further study is required to understand the model performance during more extreme geomagnetic events.

For navigation applications, the vector components of the geomagnetic field are typically expressed in terms of total field (F), declination (D) and inclination (I). The total field is the magnitude of the geomagnetic field

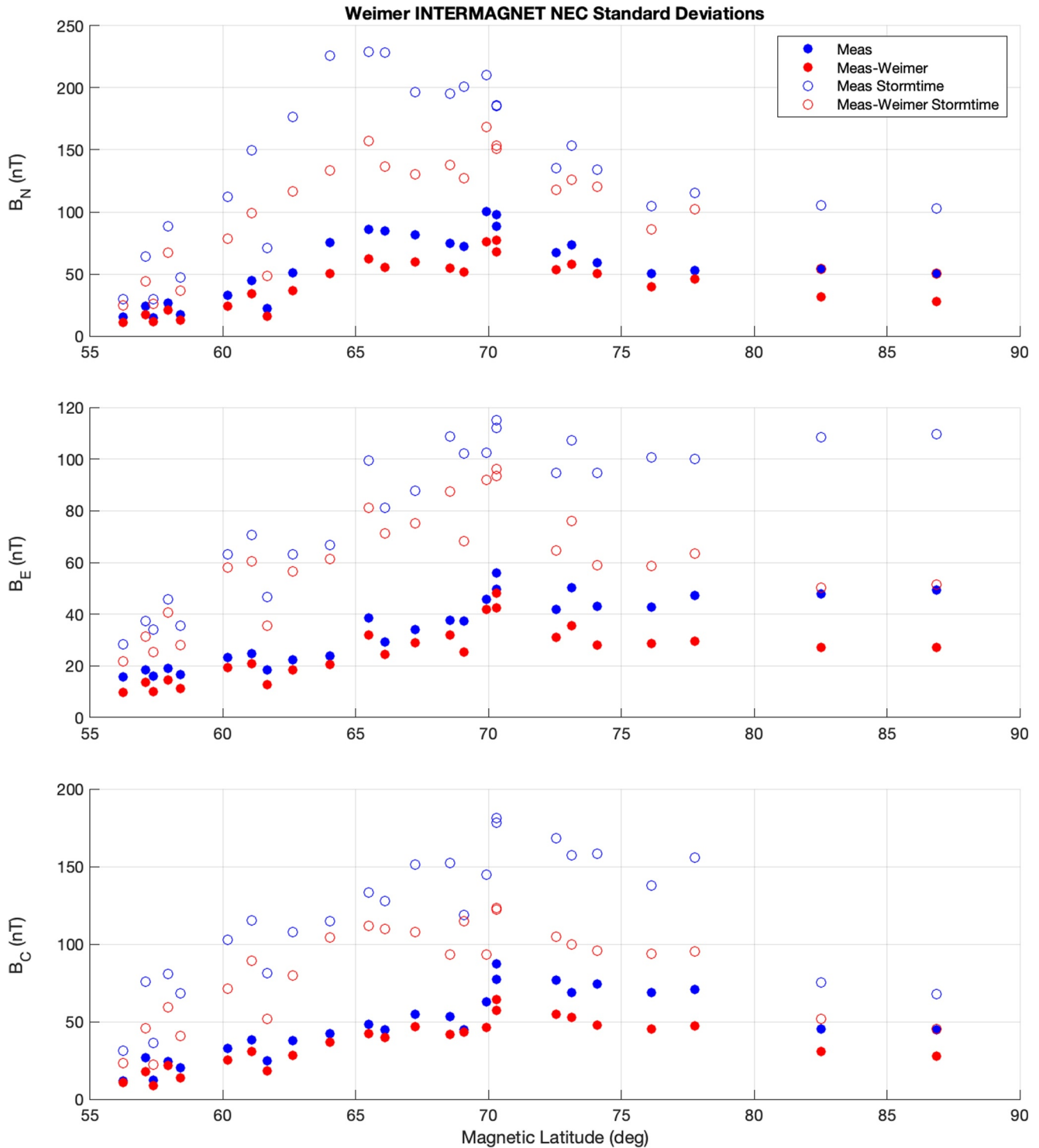


Figure 4. Standard deviations of the measurements (blue) and measurement residuals relative to WGPM (red) as a function of magnetic latitude. Results for all of the data are plotted in closed circles, and open circles represent data for $K_p \geq 4$.

$$F = \sqrt{b_N^2 + b_E^2 + b_C^2}$$

where b_N , b_E , and b_C are the North, East and Center components of the geomagnetic field, respectively. Declination is the angular difference between magnetic and true north

$$D = \tan^{-1} \left(\frac{b_E}{b_N} \right)$$

and inclination is the angle between the geomagnetic field vector and local vertical in geographic coordinates.

$$I = \sin^{-1} \left(\frac{b_C}{F} \right)$$

To evaluate the accuracy of WGPM for total field, declination and inclination, we first use the baseline geomagnetic field values determined at each observatory during quiet intervals to compute baseline F, D and I, and then compute the standard deviations of the error in F, D and I for the raw measurement and the WGPM-compensated measurement. The WGPM-compensated measurement is the difference between the measured geomagnetic variation about the baseline and the WGPM prediction. The results are shown in Figure 5 using a similar format to Figure 4. At high latitudes, the geomagnetic field tends to be more vertical, so total field variations are more strongly affected by changes in the C component. The high-latitude field geometry also causes declination errors to be larger than inclination errors, as the E and N components are smaller and are more sensitive to variations.

Figure 6 displays the ratio of the standard deviation of the WGPM-compensated data to the standard deviation of the observations. WGPM reduces the standard deviations by ~20%–30% on average, and up to 50% for some observatories. Declination errors are larger at higher latitudes because of the increased sensitivity to E and N component compensation in those locations. The relative performance of the model during geomagnetically active times is similar to the results using all of the data, although the absolute error reduction is greatest during active times given the larger variations during geomagnetic storms.

The results in Figures 4–6 indicate that WGPM typically captures 20%–30% of the variations in the data relative to an established baseline. In addition to the geomagnetic variations, there are also errors in the HDGM core and crustal magnetic field model that contribute static errors in total field, declination and inclination. These errors are associated with local geological features that cause shorter wavelength geomagnetic anomalies than the resolution of the HDGM. The HDGM 1-sigma uncertainties are 107 nT total field, 0.16° inclination and 0.3° declination (Maus et al., 2012), which are on the order of the storm-time 1-sigma variations in Figure 5. These errors represent the unmodeled parts of the Earth's crustal and core magnetic fields in the HDGM model, and we consider them to be systematic errors since they do not change from one observation to another at a specific site during a short (a week or two) period of operation. The errors due to space-weather related geomagnetic field variations are random errors since their effect can be positive or negative from observation to observation.

To account for baseline errors in the HDGM model, we define a total error as the root sum squared (RSS) of the HDGM baseline error and the variations relative to the baseline caused by geomagnetic activity (random or measurement errors), as these errors are independent. The results in Table 1 reflect the average standard deviations from the 25 INTERMAGNET observatories. When considering both quiet and active geomagnetic conditions, the one-sigma HDGM baseline errors are larger than the variations in the measurement, so the impact of WGPM is smaller. Overall, WGPM decreases total error by 3.7% in total field, 10.5% in declination, and 2.7% in inclination. During geomagnetically active times ($K_p \geq 4$), contributions to total field and inclination errors are similar between the HDGM and geophysical variations, and declination errors due to geophysical variations are approximately a factor of two greater than the HDGM model uncertainty. The active-time reduction in total error by WGPM is 15.1% for total field, 23.9% for declination and 11.4% for inclination. We note that the baseline offset in the HDGM at any given location is typically stable in the absence of active geological changes (e.g., volcanoes), so the relative impact of WGPM on total error can be improved by a magnetic survey to establish the local baseline offset.

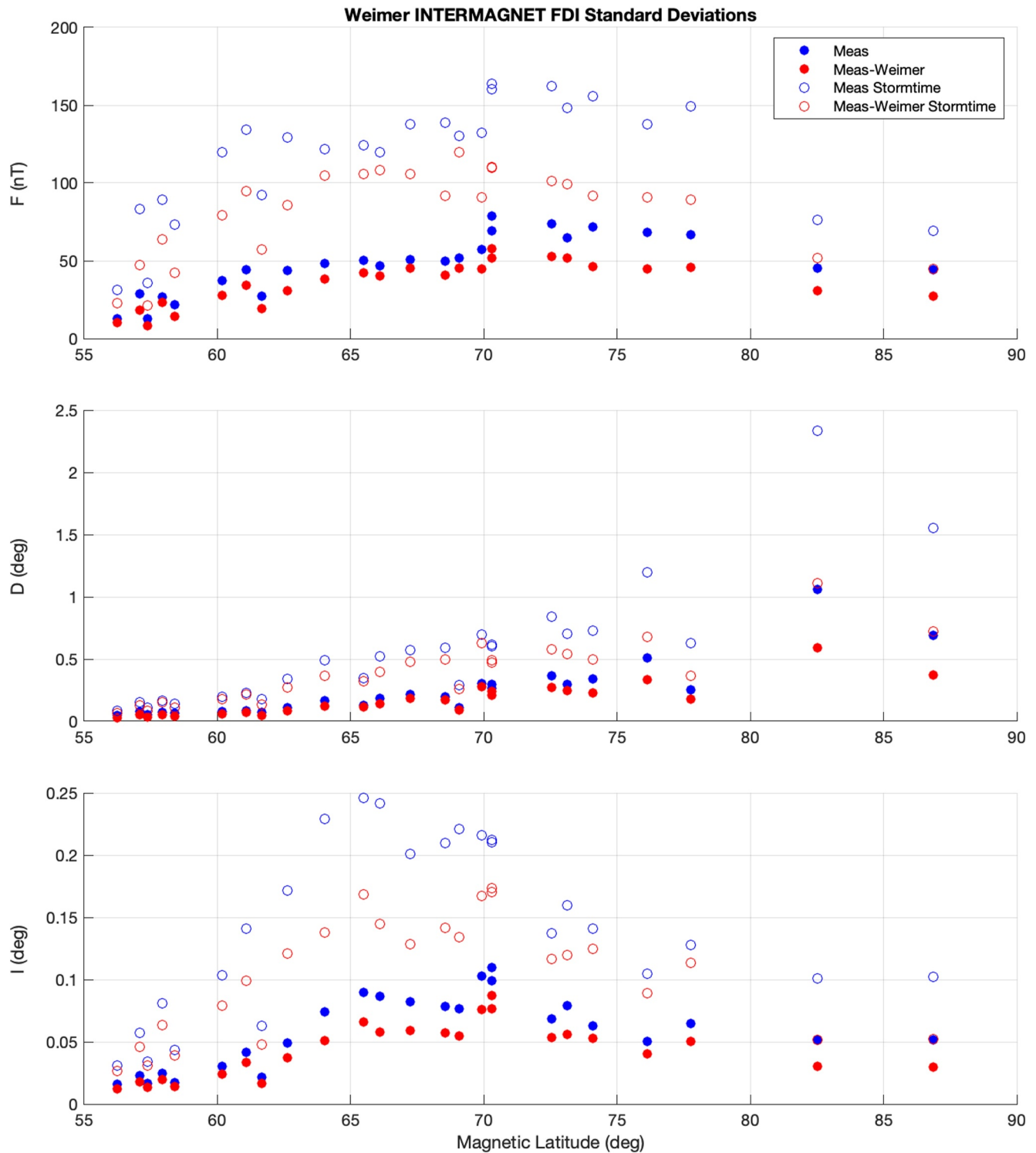


Figure 5. Standard deviations of the total field (F), declination (D) and inclination (I) errors based on the measurements (blue) and measurement with WGPM subtracted (red) as a function of magnetic latitude. Results for all of the data are plotted in closed circles, and open circles represent data for $K_p \geq 4$.

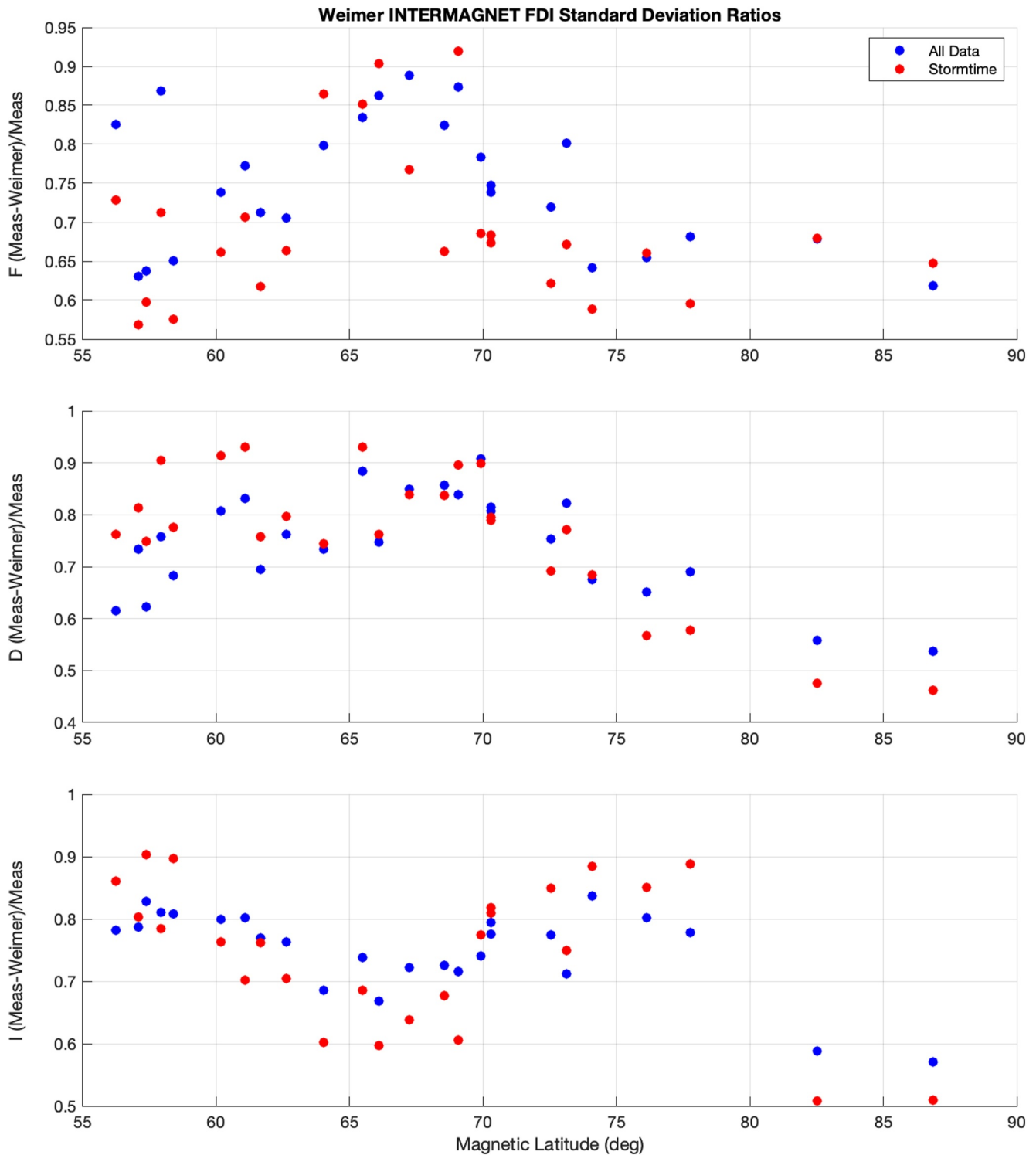


Figure 6. Ratios of standard deviations of the total field (F), declination (D) and inclination (I) errors based on the measurements compensated with WGPM relative to the raw measurements as a function of magnetic latitude. Results for all of the data are plotted in blue, and red circles represent data for $K_p \geq 4$.

Table 1
Summary of WGPM Performance Including HDGM Baseline Errors

All data						
	HDGM baseline	Measured disturbance	WGPM compensated	HDGM + measured disturbance RSS	HDGM + WGPM compensated RSS	% difference
Total Field Std. Dev. (nT)	107	47.67	35.67	117.14	112.79	3.7
Declination Std. Dev. (deg)	0.3	0.242	0.170	0.385	0.345	10.5
Inclination Std. Dev. (deg)	0.16	0.059	0.044	0.170	0.166	2.7
Kp ≥ 4						
	HDGM baseline	Measured disturbance	WGPM compensated	HDGM + measured disturbance RSS	HDGM + WGPM compensated RSS	% difference
Total Field Std. Dev. (nT)	107	116.66	81.21	158.30	134.33	15.1
Declination Std. Dev. (deg)	0.3	0.573	0.390	0.647	0.492	23.9
Inclination Std. Dev. (deg)	0.16	0.144	0.103	0.215	0.191	11.4

5. WGPM-Geospace Comparison

Here we compare the performance of the empirical WGPM to the physics-based Geospace model using data from the SuperMAG observatory network. Al Shidi et al. (2022) produced outputs for the Geospace model at SuperMAG observatory locations for 122 geomagnetic storms between 2010 and 2019. The model configuration was identical to the operational Geospace model used by NOAA SWPC. We leverage the data set from Al Shidi et al. (2022) to compare Geospace and Weimer at high latitudes for 12 geomagnetic storms during 2017–2018, which are shown in Figure 7.

The standard deviations in geographic NEC coordinates are plotted in Figure 8 for the raw observations, the residuals with respect to the Geospace model, and the residuals with respect to WGPM. The trends with magnetic latitude are similar to the trends observed in the comparison to INTERMAGNET data (Figure 4). There is a maximum in the N component variations near 60°–65° magnetic latitude, and the E and C component variations increase with magnetic latitude up to ~67°. These trends are shifted to lower latitudes by a few degrees relative to the INTERMAGNET trends in Figure 4—the Geospace comparison only uses data during geomagnetic storms, where geomagnetic disturbances tend to reach lower latitudes.

Figure 8 shows the standard deviations at each observatory for the measurement (blue), Geospace residuals (green) and the Weimer residuals (red). The Geospace standard deviations are similar to the WGPM standard deviations in the N component up to ~65° magnetic latitude, and both are lower than the measurement standard deviations, indicating that both models improve the prediction of the N component variations. However, at higher magnetic latitudes, the Geospace residuals are consistently larger than the Weimer residuals in all components, and the Geospace residuals are often larger than the raw measurement standard deviations.

The differences are more apparent in the ratios of standard deviations shown in Figure 9. A ratio of 1 means that the model-compensated data has the same standard deviation as the raw data, and a ratio greater than 1 indicates that the model increases the variance in the data, or that the model compensation would increase pointing errors in an applied setting. The WGPM results are similar to what was observed with the smaller set of INTERMAGNET observatories using 2 years of data, where the model reduces the standard deviations by ~20%–30% on average, and captures nearly 50% of the geomagnetic variation in some locations. There are some cases where WGPM increases the variation, but in general, WGPM improves the magnetic field estimate during geomagnetic storms.

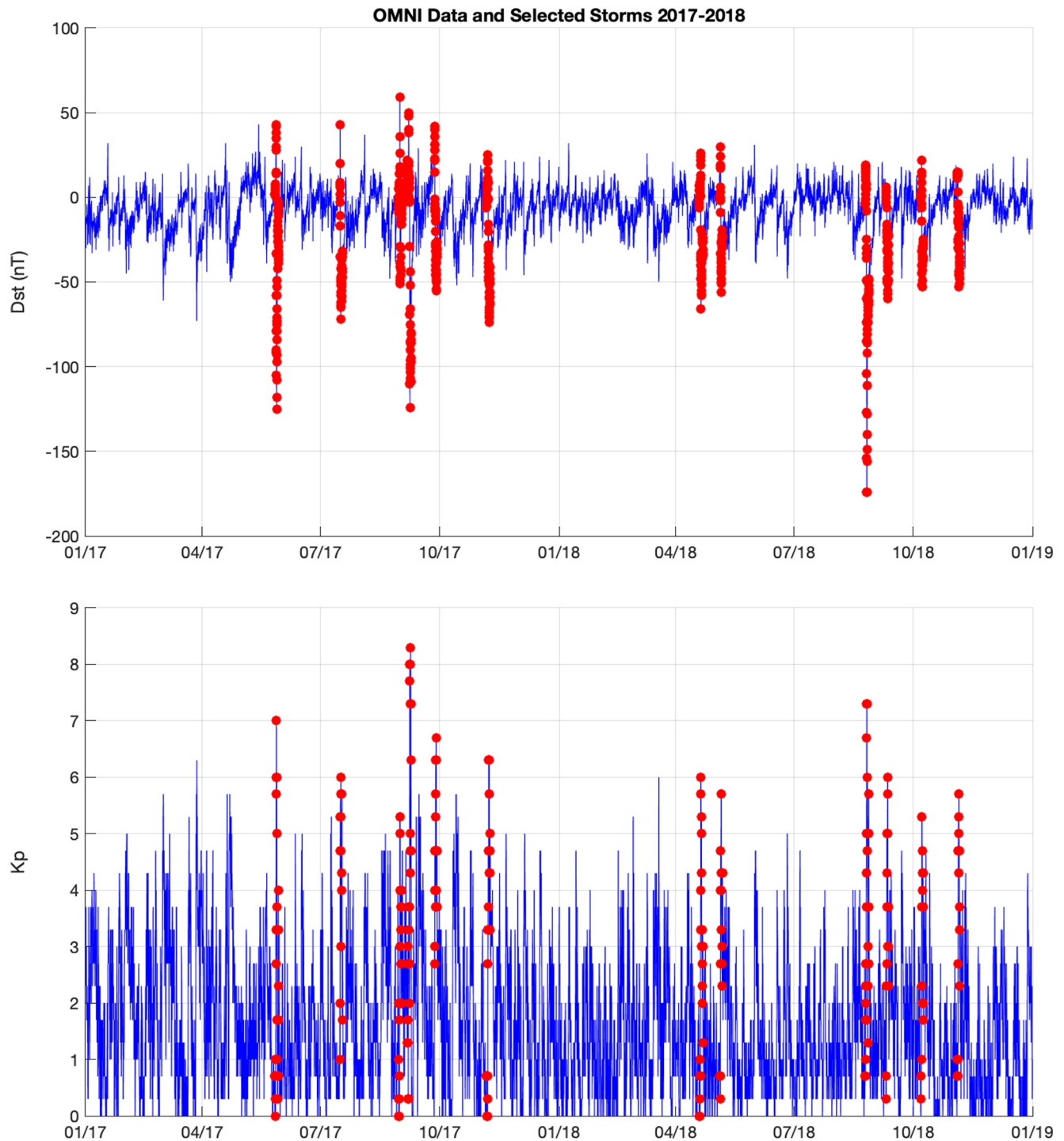


Figure 7. Dst and Kp indices for 2017 and 2018. Red markers indicate storms selected for comparison between Geospace and WGPM.

The Geospace model, on the other hand, often has ratios greater than 1, except for the E component below 70° magnetic latitude. This indicates that the Geospace model tends to overpredict geomagnetic variations.

There are several possible explanations for why the WGPM produces better predictions than the Geospace model. The Geospace model is a physics-based model that couples the outer magnetosphere, inner magnetosphere and

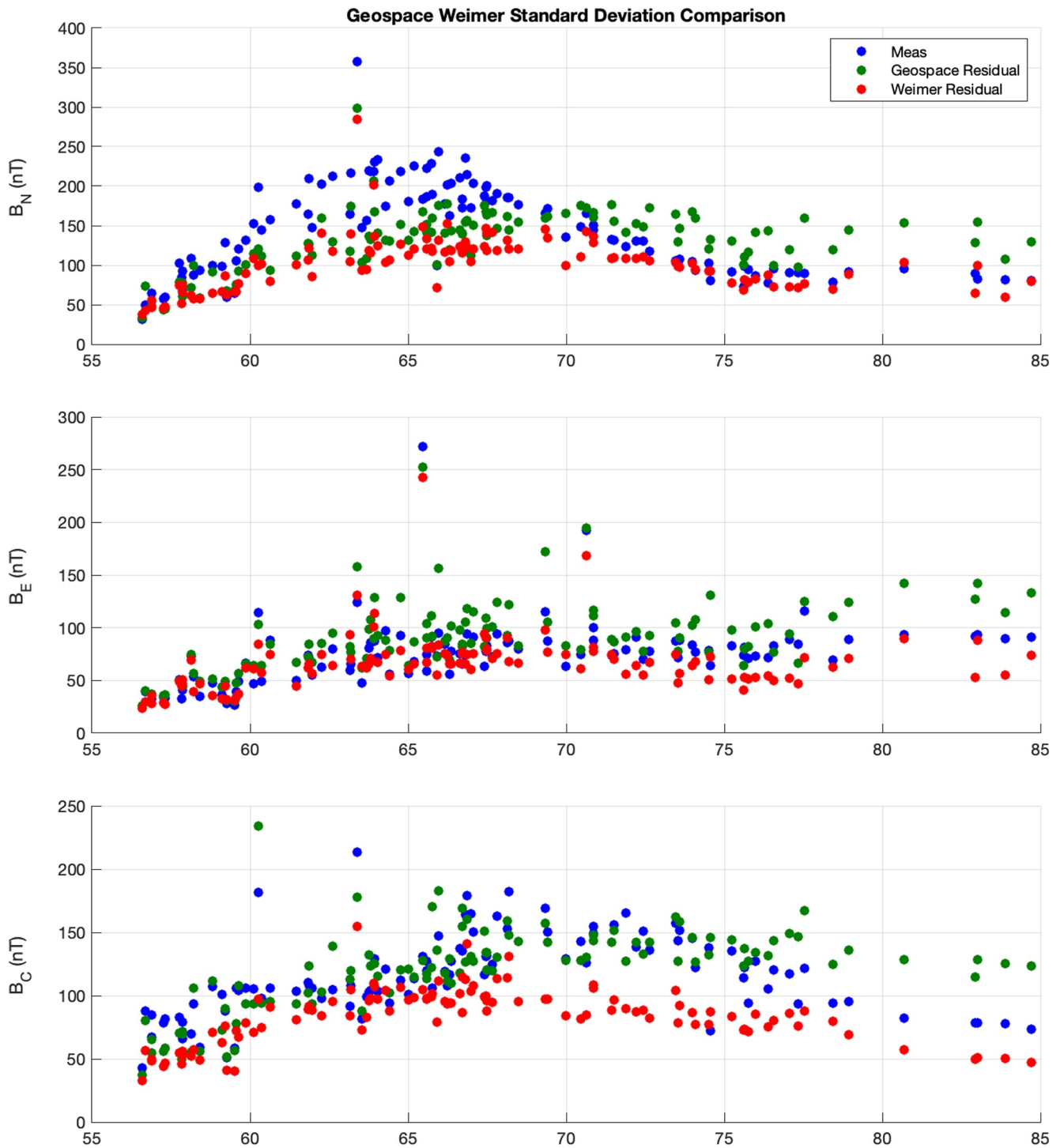


Figure 8. Standard deviations of the measurements (blue), measurement residuals relative to the Geospace model (green), and measurement residuals relative to WGPM (red) as a function of magnetic latitude.

ionosphere, and the geomagnetic perturbations predicted on the ground are based on currents in the magnetosphere and ionosphere. Coupling between the magnetosphere and ionosphere is strongly affected by ionospheric conductance. The Geospace model specifies ionospheric conductance using an empirical model (Ridley et al., 2006) that may limit the ability of the model to accurately capture the coupled magnetosphere-ionosphere

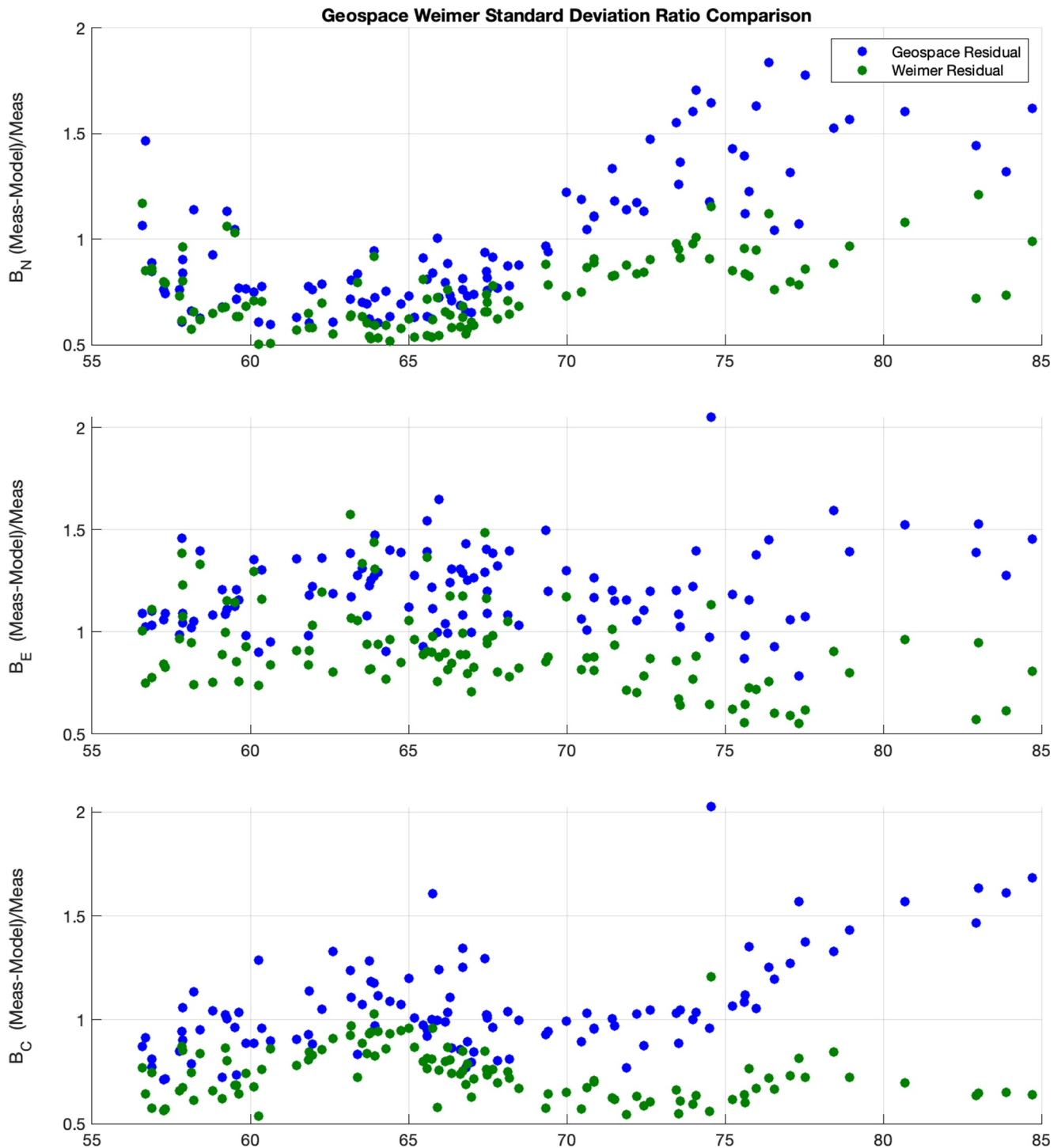


Figure 9. Ratios of standard deviations of residuals based on the measurements compensated with the Geospace model (blue) and WGPM (green) relative to the raw measurements as a function of magnetic latitude.

dynamics (Welling et al., 2017). Additionally, ground conductance is not included in the Geospace model. Ground conductance causes induced currents inside the Earth that affect the total observed perturbation on the ground by ~30% (Pulkkinen & Engels, 2005). The WGPM, on the other hand, is an empirical model developed using measured perturbations at the observatories, and the ionospheric and ground conductance effects are

implicitly included in the model. The model is parameterized by geomagnetic latitude and MLT, rather than geographic latitude and longitude, so the impact of ground conductance is globally averaged across the observatories. Additionally, the geomagnetic activity level during comparison interval was relatively quiet, and the results do not capture the model performance during more extreme geomagnetic events. The results do show that WGPM is preferable for our application during moderate activity levels.

6. Application of WGPM to Drilling Operations

In this section, we compare WGPM to MWD data collected from four high-latitude onshore and offshore sites near Prudhoe Bay in Alaska during selected geomagnetically active periods in 2017–2018. The MWD measurement stations are collected and used while drilling to determine wellbore positioning, with quality checks of the F and I measurements made against a geomagnetic reference model. If the station fails the quality check, it might be necessary to retake the measurement, which wastes valuable rig time. These measurements are affected by drill string interferences (DSI) from magnetic materials in the BHA, and the interference is compensated using Multi Station Analysis (MSA) methods that rely on the accuracy of the geomagnetic reference model. The geomagnetic model and downhole equipment accuracy is then used to determine the final wellbore position and EOU. Note that MWD cannot measure declination directly, so the declination uncertainty is driven by the uncertainty in the geomagnetic reference model.

There are five main types of geomagnetic reference models used in the directional drilling operations as per the classification by the Industry Steering Committee on Wellbore Survey Accuracy (ISCWSA <https://www.iscwsa.net/media/files/files/c23e8374/five-primary-geomagnetic-reference-model-categories-rev2.pdf>, accessed on 7 Feb 2024). Models such as HDGM are classified as High Resolution Geomagnetic Models (HRGM) and fall into a middle category in terms of their uncertainty. The most accurate reference is called In-Field Referencing—2, which includes local magnetic surveys to precisely estimate the crustal field contribution, in combination with a local, continuous measurement of space-weather signals using a field geomagnetic observatory. The HDGM can be used directly as a geomagnetic reference model, however, local crustal anomalies can create static offsets, and the dynamic geomagnetic disturbance field is not included in the model. Our application is aimed at addressing situations where there is no nearby observatory to compensate for geomagnetic disturbances.

Figure 10 shows an example of MWD data collected from 2018-08-28 to 2018-09-01, which was during the recovery phase of a large geomagnetic storm ($K_p = 7+$) on 2018-08-26. The MWD data show geomagnetic variations >400 nT and peak inclination (dip) variations $>0.35^\circ$. The Deadhorse observatory (DED, 70.4°N , 148.8°W) is located 50 km southeast from the drilling site, and the variations in total field and inclination (red line) closely follow the MWD measurements. The WGPM predictions (green line) generally follow the disturbance trends, but the model misses some of the faster transients and larger peaks. For the data shown the applying WGPM reduces the standard deviation of the total field from 96 to 76 nT (21%) and inclination from 0.096° to 0.068° (29%), which is consistent with the global statistics for WGPM. Using DED data to compensate for geomagnetic disturbances results in standard deviations of 53 nT (55%) and 0.36° (63%) for total field and inclination, respectively.

In Figure 11, total field and inclination deviations from compensated measurements using WGPM (blue) and nearby observatories (red) are plotted against raw MWD observations. The black dashed line indicates the trend where the compensated disturbance is equal to the uncompensated disturbance, and the blue and red lines are slopes fit to the data compensated by WGPM and nearby observatories, respectively. The WGPM slopes are 0.72 for total field and 0.62 for inclination, which demonstrates that WGPM can mitigate the effect of geomagnetic disturbances when applied real MWD data. Using nearby observatory data to compensate for disturbances is clearly superior to the model, but these measurements are only available in some locations. Poedjono et al. (2014) characterized the “maximum distance” between a hypothetical drilling site and a geomagnetic observatory to produce useful information for MWD geomagnetic perturbation compensation using a chain of ground observatories. They found that the observatory needs to be within 60 km of the drilling site to reduce the disturbance field error by 75%. Considering the fact that it is not always possible to have an observatory within 60 km of the drilling site, especially for offshore regions, an error reduction using a model such as WGPM is the next best option.

In addition to error reduction, WGPM will improve the station acceptance workflow, where the quality of MWD data is determined by comparing the total field and dip to the geomagnetic reference model. Figure 12 shows the difference in the Center and Horizontal field components using no compensation for the external field, the

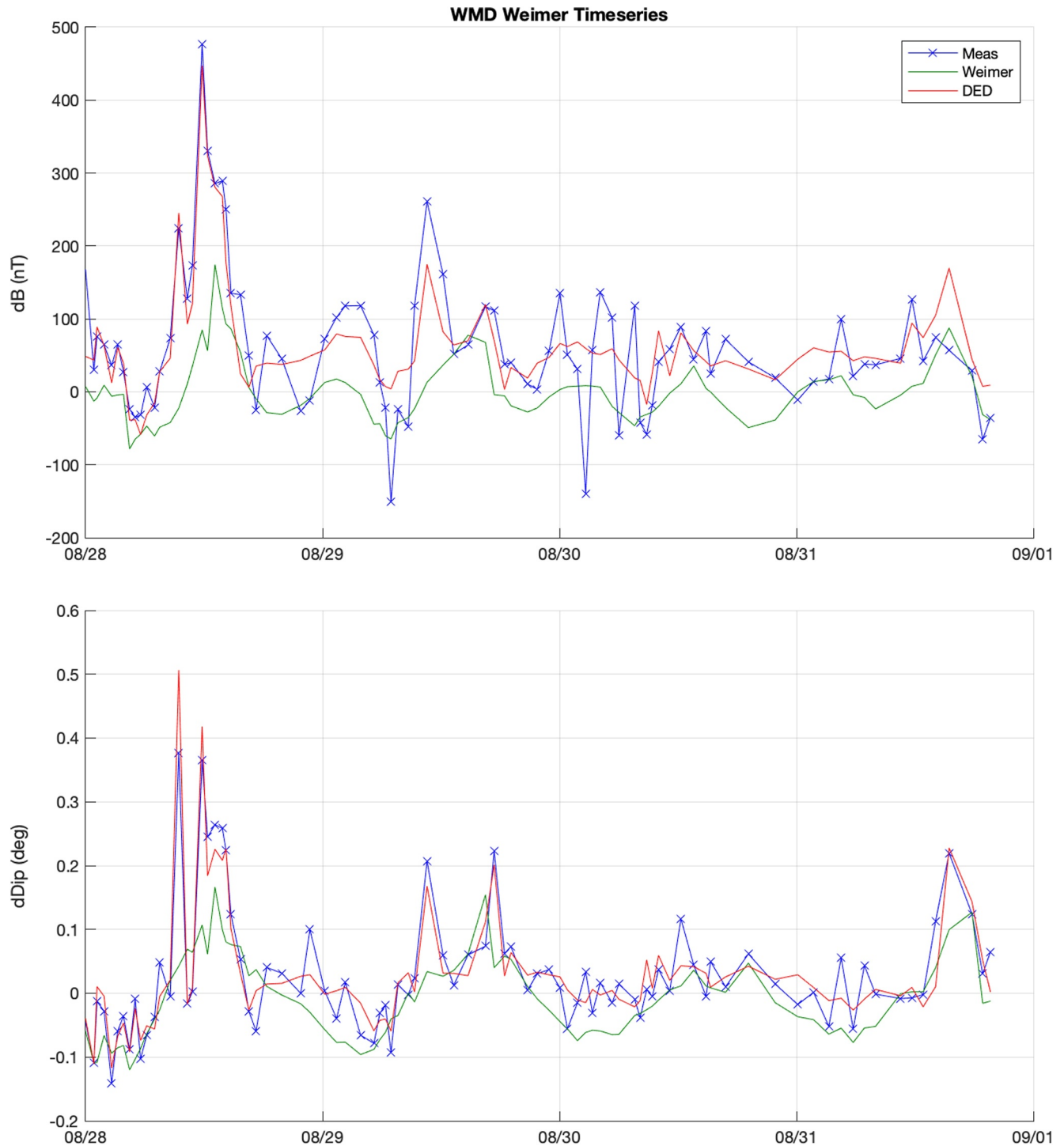


Figure 10. Variations in total field (top panel) and inclination (bottom panel) from Measurement While Drilling data (blue line) compared to Weimer (green line) and Deadhorse observatory (DED) (red line).

WGPM compensation, and the nearby observatory compensation. The dotted line shows the acceptance criteria in terms of the horizontal and center components assuming limits of 125 nT for total field and 0.25° for inclination. The acceptance pass rates are presented in Table 2. In the four wells analyzed, the quality acceptance rate for the stations was 82% when using the standard HDGM geomagnetic reference model. This means that about 1 out of

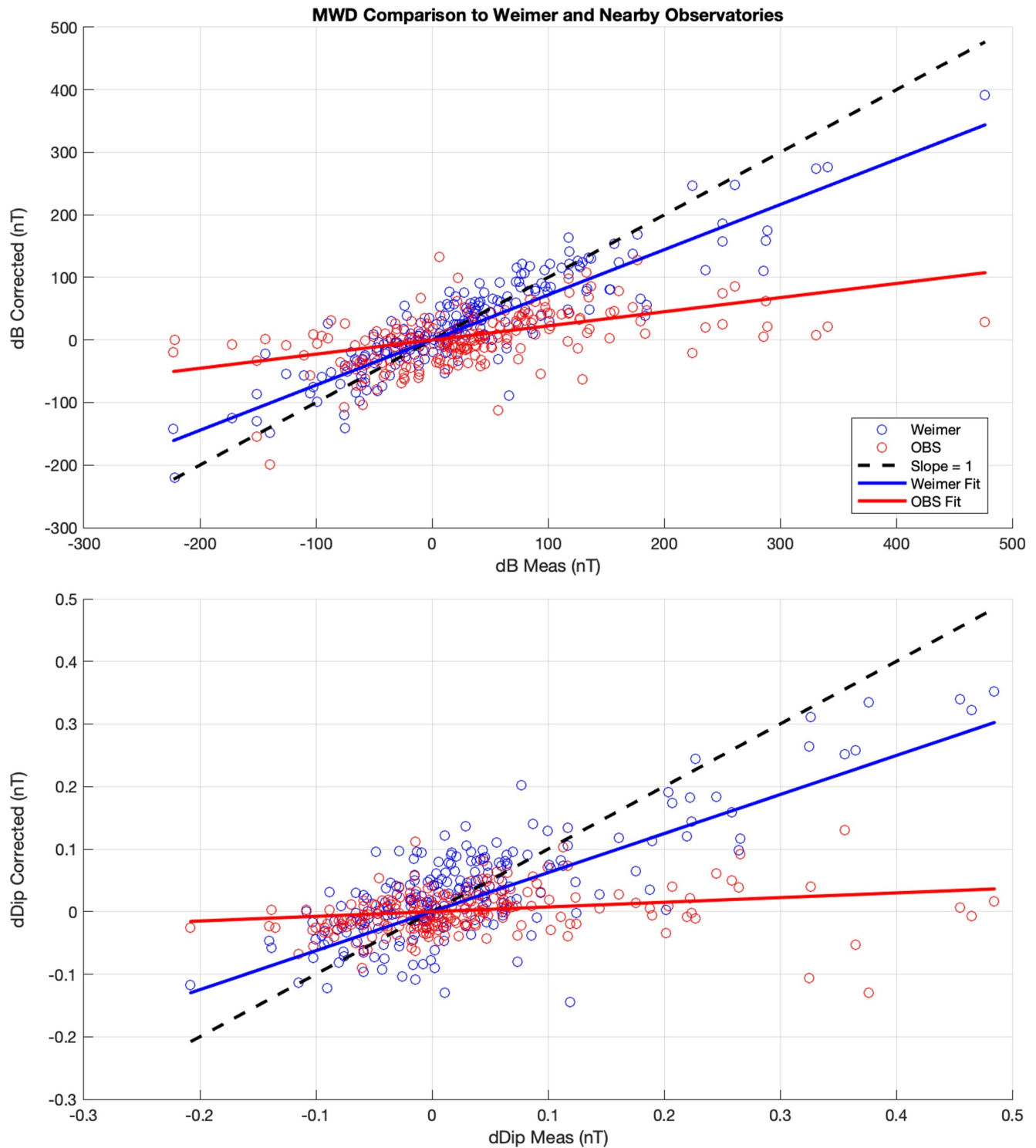


Figure 11. Variations in total field (top panel) and inclination (bottom panel). Compensated measurements are plotted against uncompensated measurements using WGPM (blue) and nearby observatories (red).

every 5 survey stations needed to be retaken to ensure their accuracy. By including WGPM to compensate for geomagnetic disturbances, this pass rate improves to 88%. Using the nearby geomagnetic observatory as the reference improves the pass rate further to 98%.

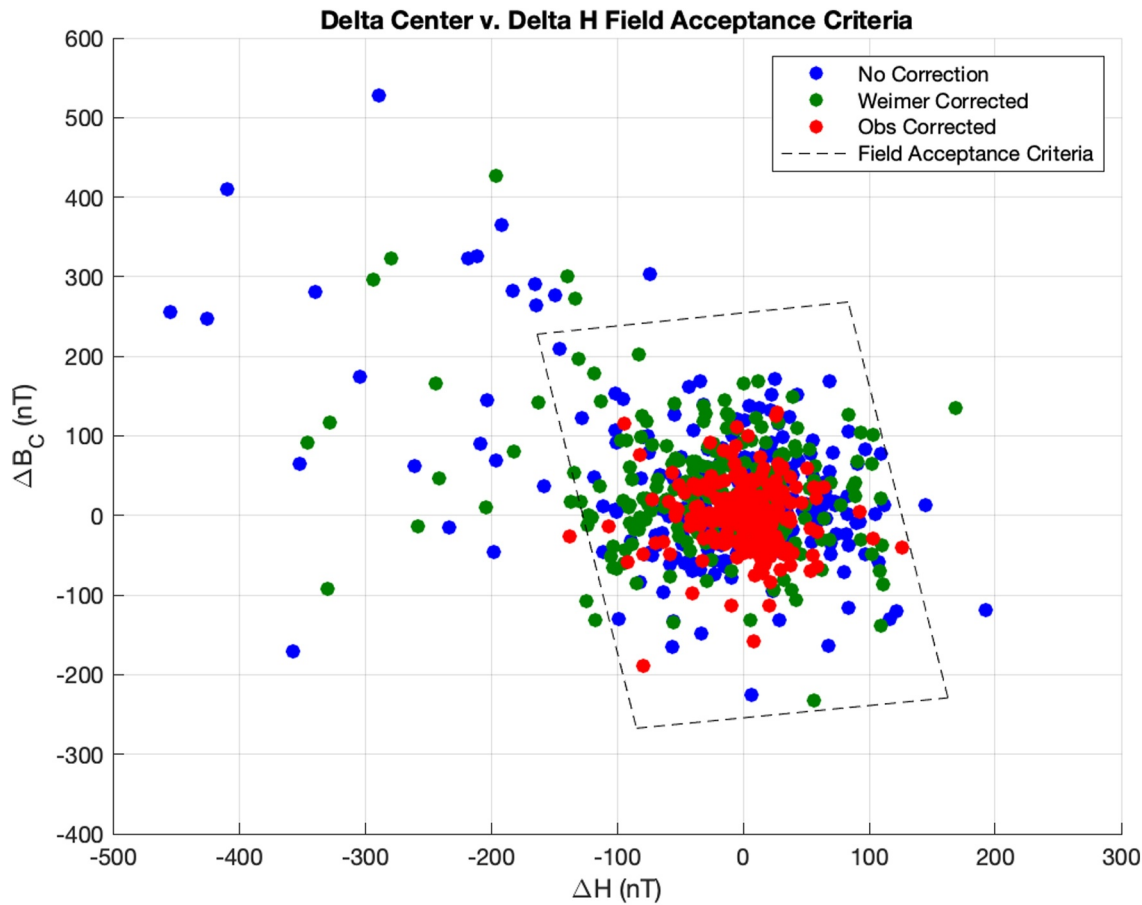


Figure 12. The difference in the Horizontal ($\sqrt{E^2 + N^2}$) and Center magnetic field components between downhole Measurement While Drilling (MWD) measurements and indicated geomagnetic reference models. A station with a value (0, 0) indicates that the MWD measured the magnetic field exactly as described by the geomagnetic model.

7. Conclusions

We evaluated WGPM at magnetic latitudes above 55° in the northern hemisphere as a candidate model for real-time prediction of magnetic field variations in NOAA's HDGM. Model predictions were compared to 25 observatory measurements from INTERMAGNET during 2017 and 2018. WGPM was found to reduce the standard deviations at the observatories by $\sim 20\%$ – 30% on average and up to $\sim 50\%$ in some locations, indicating that the model can improve real-time estimates of the magnetic field in locations where magnetic observations are not available.

When HGDM baseline errors are considered, WGPM becomes relatively less effective on average, as the magnitude of the high-latitude magnetic variations is typically smaller than the global uncertainty of the HGDM. However, during geomagnetically active times ($K_p \geq 4$), the model provides a modest improvement to the total error, reducing standard deviations by 15.1% for total field, 23.9% for declination and 11.4% for inclination on average.

Table 2
Acceptance Pass Rate Comparison

	No compensation	Weimer compensated	Obs compensated
Distance to reference mean (nT)	110.21	96.20	45.47
Distance to reference stdDev (nT)	101.12	75.95	31.73
Acceptance Criteria Pass Rate	82.19%	88.13%	98.17%

We also compared WGPM to the Geospace model during several geomagnetic storms in 2017 and 2018 using data from SuperMAG. The WGPM performance during these storms was similar to the general performance during 2017–2018. The Geospace model often increased the standard deviations at the SuperMAG observatories, which suggests that the model overpredicts geomagnetic variations, either by overpredicting the magnitude of the variations, or by predicting geomagnetic field fluctuations that did not occur.

Finally, we applied WGPM to MWD data collected from high-latitude drilling operations, and demonstrated that WGPM can reduce the impact of geomagnetic disturbances in a real-world setting. The model would be useful in settings where nearby observatory data are not available in real time.

Data Availability Statement

INTERMAGNET data can be found at www.intermagnet.org, and SuperMAG data are available at <https://supermag.jhuapl.edu>. Geospace model outputs are available from Al Shidi and Pulkkinen (2022). The Weimer magnetic perturbation model is available at Weimer (2024). Proprietary MWD data can be requested via a formal request via email to the paper authors. An NDA will then be provided for signature in order to access the data.

Acknowledgments

The results presented in this paper rely on data collected at magnetic observatories. We thank the national institutes that support them and INTERMAGNET for promoting high standards of magnetic observatory practice. This research was supported in part by NOAA cooperative agreement NA22OAR4320151, for the Cooperative Institute for Earth System Research and Data Science (CIERSDS). The statements, findings, conclusions, and recommendations are those of the authors and do not necessarily reflect the views of NOAA or the U.S. Department of Commerce.

References

- Al Shidi, Q., & Pulkkinen, T. (2022). Space Weather Modeling Framework simulations of ground magnetometer data [Dataset]. *University of Michigan - Deep Blue Data*. <https://doi.org/10.7302/dkjd-1j05>
- Al Shidi, Q., Pulkkinen, T., Toth, G., Brenner, A., Zou, S., & Gjerloev, J. (2022). A large simulation set of geomagnetic storms—Can simulations predict ground magnetometer station observations of magnetic field perturbations? *Space Weather*, 20(11), e2022SW003049. <https://doi.org/10.1029/2022sw003049>
- Anderson, C. W., III, Lanzerotti, L. J., & MacLennan, C. G. (1974). Outage of the L4 system and the geomagnetic disturbances of 4 August 1972. *Bell System Technical Journal*, 53(9), 1817–1837. <https://doi.org/10.1002/j.1538-7305.1974.tb02817.x>
- Bartels, J. (1949). The standardized index, Ks, and the planetary index, Kp. *IATME Bull*, 12b, 97–120.
- Boteler, D. H., Pirjola, R. J., & Nevanlinna, H. (1998). The effects of geomagnetic disturbances on electrical systems at the Earth's surface. *Advances in Space Research*, 22(1), 17–27. [https://doi.org/10.1016/s0273-1177\(97\)01096-x](https://doi.org/10.1016/s0273-1177(97)01096-x)
- Buchanan, A., Finn, C. A., Love, J. J., Worthington, E. W., Lawson, F., Maus, S., & Poedjono, B. (2013). Geomagnetic referencing—The real-time compass for directional drillers. *Oilfield Review*, 25(3), 32–47.
- Chulliat, A., Vigneron, P., & Hulot, G. (2016). First results from the Swarm dedicated ionospheric field inversion chain. *Earth Planets and Space*, 68(1), 104. <https://doi.org/10.1186/s40623-016-0481-6>
- Gjerloev, J. W. (2012). The SuperMAG data processing technique. *Journal of Geophysical Research*, 117(A9), A09213. <https://doi.org/10.1029/2012JA017683>
- Gombosi, T. I., Powell, K. G., De Zeeuw, D. L., Clauer, C. R., Hansen, K. C., Manchester, W. B., et al. (2004). Solution-adaptive magnetohydrodynamics for space plasmas: Sun-to-Earth simulations. *Computing in Science & Engineering*, 6(2), 14–35. <https://doi.org/10.1109/mcise.2004.1267603>
- Kerridge, D. (2001). INTERMAGNET: Worldwide near-real-time geomagnetic observatory data. In *Proceedings of the workshop on space weather* (Vol. 34). ESTEC.
- Macmillan, S., & Olsen, N. (2013). Observatory data and the Swarm mission. *Earth Planets and Space*, 65(11), 1355–1362. <https://doi.org/10.5047/eps.2013.07.011>
- Maus, S., & Lühr, H. (2005). Signature of the quiet-time magnetospheric magnetic field and its electromagnetic induction in the rotating Earth. *Geophysical Journal International*, 162(3), 755–763. <https://doi.org/10.1111/j.1365-246X.2005.02691.x>
- Maus, S., Nair, M. C., Poedjono, B., Okewunmi, S., Fairhead, J. D., Barckhausen, U., et al. (2012). High definition geomagnetic models: A new perspective for improved wellbore positioning. In *IADC/SPE drilling conference and exhibition*. <https://doi.org/10.2118/151436-MS>
- Nair, M., Chulliat, A., Woods, A., Alken, P., Meyer, B., Poedjono, B., et al. (2021). Next generation high-definition geomagnetic model for wellbore positioning, incorporating new crustal magnetic data. In *Paper presented at the offshore technology conference, virtual and Houston*. Paper Number: OTC-31044-MS. <https://doi.org/10.4043/31044-MS>
- Olsen, N., Lühr, H., Finlay, C. C., Sabaka, T. J., Michaelis, I., Rauberg, J., & Tøffner-Clausen, L. (2014). The CHAOS-4 geomagnetic field model. *Geophysical Journal International*, 197(2), 815–827. <https://doi.org/10.1093/gji/ggu033>
- Poedjono, B., Maus, S., & Manoj, C. (2014). Effective monitoring of auroral electrojet disturbances to enable accurate wellbore placement in the Arctic. In *Paper presented at the OTC Arctic technology conference*. <https://doi.org/10.4043/24583-MS>
- Pulkkinen, A., & Engels, M. (2005). The role of 3-D geomagnetic induction in the determination of the ionospheric currents from the ground geomagnetic data. In *Annales geophysicae* (Vol. 23(3), pp. 909–917). <https://doi.org/10.5194/angeo-23-909-2005>, Copernicus Publications.
- Pulkkinen, A., Rastätter, L., Kuznetsova, M., Singer, H., Balch, C., Weimer, D., et al. (2013). Community-wide validation of geospace model ground magnetic field perturbation predictions to support model transition to operations. *Space Weather*, 11(6), 369–385. <https://doi.org/10.1002/swe.20056>
- Pulkkinen, A., Viljanen, A., & Pirjola, R. (2006). Estimation of geomagnetically induced current levels from different input data. *Space Weather*, 4(8), S08005. <https://doi.org/10.1029/2006SW000229>
- Ridley, A. J., Deng, Y., & Toth, G. (2006). The global ionosphere–thermosphere model. *Journal of Atmospheric and Solar-Terrestrial Physics*, 68(8), 839–864. <https://doi.org/10.1016/j.jastp.2006.01.008>
- Ridley, A. J., Gombosi, T. I., & DeZeeuw, D. L. (2004). Ionospheric control of the magnetosphere: Conductance. In *Annales geophysicae*, (Vol. 22(2), pp. 567–584). <https://doi.org/10.5194/angeo-22-567-2004>, Copernicus GmbH.
- Toffoletto, F., Sazykin, S., Spiro, R., & Wolf, R. (2003). Inner magnetospheric modeling with the Rice convection model. *Space Science Reviews*, 107, 175–196. https://doi.org/10.1007/978-94-007-1069-6_19

- Weimer, D. (2024). Weimer 2013 magnetic perturbation model for IDL. In *Space weather* (Vol. 11, pp. 107–120). Zenodo. <https://doi.org/10.5281/zenodo.11151259>
- Weimer, D. R. (2005). Improved ionospheric electrodynamic models and application to calculating joule heating rates. *Journal of Geophysical Research*, 110(A5), A05306. <https://doi.org/10.1029/2004JA010884>
- Weimer, D. R. (2013). An empirical model of ground-level geomagnetic perturbations. *Space Weather*, 11(3), 107–120. <https://doi.org/10.1002/swe.20030>
- Weimer, D. R., Clauer, C. R., Engebretson, M. J., Hansen, T. L., Gleisner, H., Mann, I., & Yumoto, K. (2010). Statistical maps of geomagnetic perturbations as a function of the interplanetary magnetic field. *Journal of Geophysical Research*, 115(A10), A10320. <https://doi.org/10.1029/2010ja015540>
- Welling, D. T., Anderson, B. J., Crowley, G., Pulkkinen, A. A., & Rastätter, L. (2017). Exploring. Predictive performance: A reanalysis of the geospace model transition challenge. *Space Weather*, 15(1), 192–203. <https://doi.org/10.1002/2016SW001505>
- Welling, D. T., Ngwira, C. M., Opgenoorth, H., Haiducek, J. D., Savani, N. P., Morley, S. K., et al. (2018). Recommendations for next-generation ground magnetic perturbation validation. *Space Weather*, 16(12), 1912–1920. <https://doi.org/10.1029/2018sw002064>
- Yamazaki, Y., & Maute, A. (2017). Sq and EEJ—A review on the daily variation of the geomagnetic field caused by ionospheric dynamo currents. *Space Science Reviews*, 206(1–4), 299–405. <https://doi.org/10.1007/s11214-016-0282-z>